Paper No.
19309

AMPP ANNUAL CONFERENCE + EXPO
MARCH 19-23, 2023 | DENVER, COLORADO

Effect of Cementite on the Corrosion Inhibition of Carbon Steel with Tetradecyl Phosphate Ester in CO_2 environment

Shuai Ren, Xi Wang, David Young, Marc Singer
Institute for Corrosion and Multiphase Technology
Department of Chemical and Biomolecular Engineering
Ohio University
342 West State Street
Athens, OH 45701, USA

Maalek Mohamed-Said, Gregory Moulie, Mioara Stroe
TotalEnergies
OneTech - CSTJF, Avenue Larribau
F-64018 Pau, France

ABSTRACT

Despite extensive use of corrosion inhibitors (CIs) to mitigate internal pipeline corrosion, few studies address how corrosion residue or products affect their performance. In the present work, in-house synthesized CI model compound, tetradecyl phosphate ester (PE-C14), was used to investigate the effect of cementite (Fe_3C) on corrosion inhibition performance on C1018 steel with ferritic-pearlitic microstructure, on which residual Fe_3C skeleton tended to stay on the surface during pre-corrosion. A 40 μm Fe_3C skeleton was exposed and maintained on specimen surface after 2-day pre-corrosion under studied condition. The corrosion rata (CR) evolution results indicated that the residual Fe_3C skeleton decreased significantly the inhibition efficiency (IE) of PE-C14, with 300 ppm_w being insufficient to obtain an acceptable IE. Some caveats related to the testing protocols are discussed. Under condition of maintained Fe_3C, from the polarization curves, corrosion rate and limiting current of H^+ reduction reaction were significantly accelerated due to the Fe_3C layer supporting excessive cathodic reaction. With a *ca.* 40 μm Fe_3C layer, the retardation on anodic reaction with 300ppm_w PE-C14 is very limited compared with that on bare surface. After adding PE-C14, a non-uniform corrosion morphology was observed on specimens with 2-day pre-corrosion, which could be postulated to promote localized attack. Two main limits to the above results are identified: the experiments were conducted in close medium where the inhibitor concentration of the bulk could easily be depleted and the obtained data can only be applied in case a 40 μm thick layer of cementite is formed. These two factors have a significant effect on the outcome and further tests and work are ongoing to address these limitations.

Keywords: Corrosion inhibition, phosphate ester, iron carbide, cementite, inhibition efficiency, inhibitor complexation, localized corrosion, potentiodynamic polarization, SEM

INTRODUCTION

Internal corrosion of pipelines associated with oil and gas production and refinery has always been a challenge for corrosion engineers.[1] Over the past decades, corrosion engineers have made significant progress in developing mitigation approaches to protect these carbon steel pipelines by using corrosion inhibitors (CIs), corrosion resistant materials, and various cleaning techniques. Among all these mitigation strategies, corrosion inhibitors are considered as the first choice in handling the internal corrosion of pipelines.

Despite the extensive use of organic corrosion inhibitors in the oil and gas industry, few studies consider the role of corrosion residue or products ($Fe_3C/FeCO_3/Fe_xS_y/Fe_xO_y$) layers on inhibitor performance.[2–5] Corrosion residues or products are exposed or formed due to electrochemical corrosion reactions on the internal surfaces of pipelines. Under laboratory conditions, performance studies of corrosion inhibitors are usually conducted on carbon steel specimens with freshly polished surfaces (no corrosion residue or products). However, the internal surface of a pipeline is never as clean in actual operation. Some researchers[2–5] started to consider the effect of residual Fe_3C exposed during pre-corrosion. Many of them[2–4] have reported that residual Fe_3C has a detrimental effect on inhibitor performance by serving as a source of additional cathodic sites. However, the associated inhibition mechanism in the presence of Fe_3C is still unclear. Besides, the extent of this detrimental effect varies with different types of corrosion inhibitor and steel (carbon content and microstrcuture). Consequently, more relevant research works are required to understand the inhibition mechanism influenced by Fe_3C, which enables to evaluate this detrimental effect associated with additional Fe_3C area quantitatively. The present work studied the effect of Fe_3C on the corrosion inhibition of C1018 with tetradecyl phosphate ester (PE-C14) in CO_2 environment to gain more insights about this detrimental effect. C1018 steel is chosen explicitly because of its ferritic-pearlitic microstructure and the coherent structure (or skeleton) of cementite residue that is left behind as a result of corrosion. It should be mentioned that pipelines are often made of API-X65 (X65), which holds a lower carbon content compared to C1018 and a microstructure closer to tempered martensite or ferrite with small cementite precipitates. In the case of X65, cementite residues usually do not form a well ordered network, as on C1018. This comment should put in perspective when analyzing the results of this study. Phosphate ester-type corrosion inhibitors, as anionic surfactants, have wide applications in oil and gas production and refineries environments.[6] The tetradecyl phosphate ester (PE-C14) used in this work was synthesized in-house and its synthesis, purification, and characterization are described elsewhere.[7–12] It showed an excellent inhibition performance at the temperature range of 25 to 80 °C with a special inhibition behavior at elevated temperatures (55 to 80 °C).[7, 8, 10]

EXPERIMENTAL SETUP AND METHODOLOGY

Materials and Chemicals

Steel specimens used for electrochemical measurements were machined from UNS G10180 [(1)] carbon steel (C1018) with a ferritic-pearlitic microstructure, as shown in Figure 1. The composition of PE-C14 consists of 73.5% monoester and 26.5% diester. Their molecular structures are shown in Figure 2. The efforts to measure the concentration of PE-C14 *via* molybdenum blue method was not rewarded due to the complexity of de-esterification process in harsh condition.

[(1)] UNS numbers are listed in *Metals and Alloys in the Unified Numbering System*, published by the Society of Automotive Engineers (SAE International) and cosponsored by ASTM International.

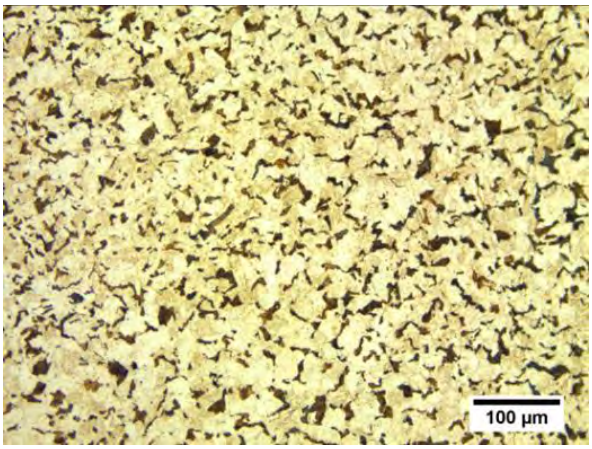

Figure 1: Ferritic-pearlitic microstrcutrue of C1018 steel used in this work.*

Figure 2: Molecular structures of in-house synthesized tetradecyl phosphate ester (PE-C14)

Experimental Setup and Matrix

The electrochemical measurements were carried out using a glass cell with an impeller and connected to a ferrous ion concentration controller *via* a flow loop, as shown in Figure 3. A detailed introduction about this setup has been reported elsewhere.[13, 14] It allows up to 7 specimens being exposed in the test environment including working electrodes and specimens for weight loss measurement and surface analysis. Meanwhile, it gives superior control of species diffusion in the electrolyte by an impeller. All specimens, at the same radial distance from the impeller, experienced identical flow conditions, *i.e.*, the same mass transfer coefficient and shear stress. The mass transfer correlation for impeller created flow in this setup was determined and shown in the following equation.

$$\mathrm{Sh} = 2.94\mathrm{Re}^{0.55}\mathrm{Sc}^{0.33}$$

* Image courtesy to Bernardo Santos, ICMT, Ohio University

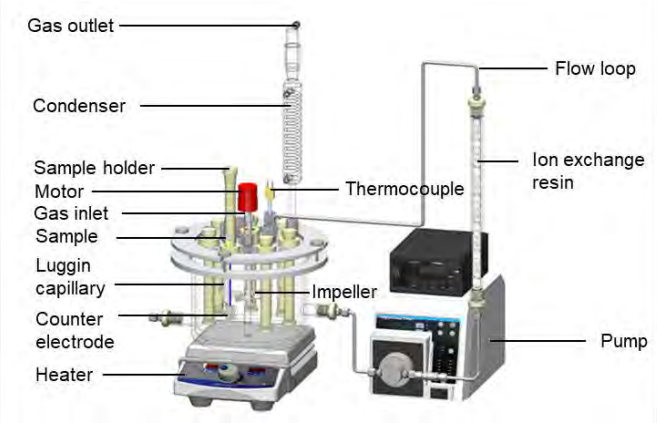

Figure 3: Schematic of the glass cell with impeller (left) and ferrous ion controller (right)†

A three-electrode configuration was adopted in this glass cell for electrochemical experiments, with a platinum grid as a counter electrode and a saturated KCl Ag/AgCl reference electrode. Two working electrodes were employed, and electrochemical measurements were conducted on them alternately *via* a Multiplexer (ECM8™, Gamry‡) connected to a potentiostat (Interface 1010, Gamry‡).

The full experimental matrix has been listed in Table 1. All the experiments were conducted at 55°C in a simulated exploration and production (EP) environment (50 g/L NaCl, 0.86 bar CO_2, pH 4.5). Two concentrations of PE-C14, *i.e.* 30 and 300 ppm_w, were selected in present work. 30 ppm_w is just higher than the surface saturation concentration (10 to 20 ppm_w),[7, 8, 10] while 300 ppm_w is at least 15 times higher than the surface saturation concentration. Prior to each experiment, all the specimens were polished up to 600 grit abrasive papers in isopropanol flow, cleaned with isopropanol in an ultrasonic bath after polishing, and air-dried before insertion into the cell. The rotational speed of the impeller was set at 52 rpm throughout these experiments, which would create the same mass transfer coefficient as flow of 1.61 m/s in a pipe with an inner diameter of 0.1m and a shear stress of 4.7 Pa. PE-C14 was pre-dissolved in isopropyl alcohol and then this mixture was deoxygenated with N_2 and injected into the bulk test solution.

Table 1
Experimental matrix of C1018 steel with PE-C14 in the presence of Fe_3C layer.

Description	Values	
Working solution	50 g/L NaCl (3 liters)	
Material	C1018	
Working electrode	Flat, 1.61 cm^2	
Immersion specimens	Flat, 1.61 cm^2	
Temperature	55 ± 2 °C	
Total pressure	1 bar	
CO_2 partial pressure	0.86 bar (saturated)	
pH	4.5 ± 0.1	
Rotational speed of impeller	52 rpm	
Inhibitor model compound: PE-C14	30 ppm_w	300 ppm_w

† Image courtesy of Cody Shafer, ICMT, Ohio University.

‡ Trade name

Experimental Procedure and Techniques

The experimental procedure is displayed in Figure 4. After two hours solution sparging with CO_2, one working electrode (WE #1) and five specimens for weight loss measurements and surface analysis were inserted into the solution. These specimens were pre-corroded for 2 days and one of the specimens was then extracted to confirm the thickness of exposed Fe_3C layer *via* cross-sectional SEM imaging. Meanwhile, a second working electrode (WE #2) without pre-corrosion was introduced into the glass cell. Then, PE-C14 was injected into the solution for inhibition tests lasting 1 to 4 days, throughout which, open circuit potential (OCP) and linear polarization resistance (LPR) measurements were conducted every hour. Meanwhile, immersed specimens were periodically extracted from solution for weight loss and surface analysis after different immersion durations. In the end, potentiodynamic polarization was executed on both working electrodes.

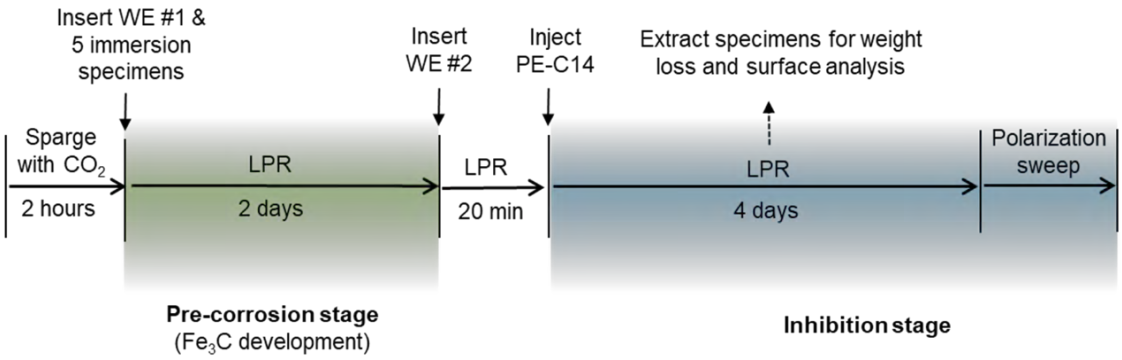

Figure 4: The schematic procedure for inhibition experiments of C1018 steel with PE-C14 in the presence of Fe_3C layer.

LPR scan range was from –5 mV to +5 mV *vs.* OCP with a scan rate of 0.125 mV/s, and a B value of 26 mV/dec was adopted to extract the corrosion rate *via* Stern-Geary equation. This value is widely used in CO_2 corrosion of mild steel.[15] The same B value was used in the presence of corrosion inhibitor for consistency purposes but also considering that the Tafel slopes did not seem to be significantly affected. Yet, it should be mentioned that a review of the validity of the chosen B value should be systematically conducted. Potentiodynamic polarization sweeps were conducted at a scan rate of 0.125 mV/s. Retrieved immersion specimens were rinsed by deionized water and isopropyl alcohol, and then air-dried before conducting top view SEM and EDS analysis. To characterize the cross-sections of these specimens, they were mounted in epoxy, finished with a fine polish using 0.25 µm diamond suspension, and sputter coated with a thin layer of palladium. The secondary electron images and EDS data were taken with an accelerating voltage of 15 kV, working distance of 14 to 15mm, and spot size of 50 to 60.

EXPERIMENTAL RESULTS AND DISCUSSION

Corrosion Rate Evolution

The corrosion rates over time of C1018 with and without 2-day pre-corrosion in studied condition at 55°C with 30 and 300 ppm_w PE-C14 are displayed in Figure 5. During 2-day pre-corrosion, the corrosion rates kept increasing to around 12 mm/year due to the acceleration by the exposed Fe_3C layer serving as additional cathodic reaction area. After 2-day pre-corrosion, a *ca.* 40 µm Fe_3C skeleton was exposed on specimen surface, verified by the cross-sectional SEM image in Figure 6d. This Fe_3C skeleton is mechanically relatively weak but a previous study has shown that a Fe_3C thickness of 40 µm can sustain a shear stress of 20 Pa.[16]

In the case of 30 ppm_w PE-C14, the corrosion rate of the specimen, which experienced 2-day pre-corrosion, decreased slightly and then stabilized around 8.0 mm/year after PE-C14 injection. However, the stabilized corrosion rate increased again after one day gradually to the same level before adding PE-C14 (12.0 mm/year), which implied the limited inhibition initially conferred was totally lost. For specimen without 2-day pre-corrosion in the same solution, the corrosion rate sharply decreased to approximately 0.2 mm/year and a high inhibition efficiency (IE) was achieved due to its lack of excess Fe_3C surface areas. However, this low corrosion rate maintained for only one day and gradually increased during the next 3 days as well. The consistency of corrosion rate trends between two specimens regardless of pre-corrosion proved there was an insufficient amount of PE-C14 in the system after 3-day of this inhibition experiment. One of the reasons proved by a separate experiment is the depletion of PE-C14 by corrosion-released Fe^{2+} *via* complexation,[17] which is beyond the scope of this work and will not be discussed in details here[§].

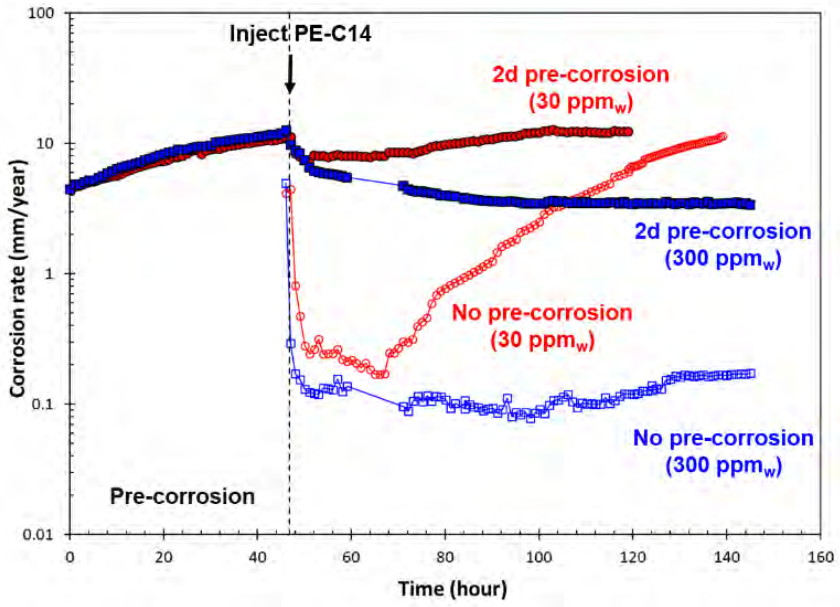

Figure 5: Corrosion rates over time for C1018 with and without 2-day pre-corrosion in 50 g/L NaCl solution with 0.86 bar CO_2 at pH 4.5 and 55 °C with 30 and 300 ppm_w PE-C14.

In the case of 300 ppm_w PE-C14, the corrosion rate after 2-day pre-corrosion decreased after injecting 300 ppm_w PE-C14 and then stabilized around 3.4 mm/year after 4-day inhibition. For the specimen without pre-corrosion, the corrosion rate quickly decreased to around 0.1 mm/year and then maintained for the remaining 4 days. It is obvious that 300 ppm_w PE-C14 still cannot inhibit the corrosion of 2-day pre-corroded C1018 to a sufficiently low level (~0.1 mm/year). However, unlike the 30 ppm_w experiment, the inhibition effect was maintained for at least 4 days on both specimens, even though, as previously postulated, PE-C14 was being consumed by Fe^{2+} during this process as well.

In comparison of the cases with and without 2-day pre-corrosion, it is concluded that the presence of a *ca.* 40 µm Fe_3C skeleton largely impaired the inhibition performance of PE-C14 in studied environment

§ The complexation of phosphate ester corrosion inhibitor with released ferrous iron could be due to the fact that the tested CI contains only phosphate ester and is a “model CI compound”. There are ongoing works to further assess this complexation using phosphate ester based commercial corrosion inhibitors.

for both concentrations. The IE with 300 ppm_w PE-C14 decreased dramatically from 97.8% on a bare surface to 28.1% on a surface with a *ca.* 40 µm Fe_3C layer.

These results should be considered with great cautiousness, and the following limitations are identified:

- The tests were conducted with ferritic-pearlitic microstructure specimen where a layer of 40 µm has been maintained. Further tests with tempered-martensite type microstructure (API 5L X65)[2, 18, 19] widely used for pipelines and known to lead to less cementite skeleton are under investigations. Also, conditions under which a layer of cementite can be maintained over longer time period need to be documented to contextualize effect of cementite and derive practical consequences. This should include effect of flow[16, 20] and/or regular cleaning of the pipeline.

- The experiments were conducted in closed glass cell with one shot of CI injection in a closed volume. In this configuration the consumption of bulk CI, through adsorption at the porous cementite network and other interfaces, is not prevented and not representing of actual pipeline conditions where CI is continuously injected.

- The above results are obtained with model CI compound and evidence of complexation between the main active compound and the released ferrous iron has been shown. This further limits the amount of available CI molecules in the bulk.

Specimen Surface Analysis

Inhibition with 30 ppm_w PE-C14.

The top and cross-sectional view of SEM images of C1018 specimens retrieved at different stages of the experiment are shown in Figure 6. After 2-day pre-corrosion, a skeletal Fe_3C structure remained on the steel surface after the dissolution of ferrite, as shown in Figure 6a and 6d. The Fe_3C thickness measured from the cross-sectional view SEM image was *ca.* 40 µm. After 2-day pre-corrosion and 1-day inhibition, the top view SEM image (Figure 6b) shows different appearance of Fe_3C layer from that after 2-day pre-corrosion only. This will be explained in detail in the EDS section. The cross-sectional SEM image (Figure 6e) demonstrates two corrosion stages according to its corrosion morphologies, *i.e.*, 2-day pre-corrosion and 1-day inhibition. The outer cementite layer was produced during the 2-day pre-corrosion stage, while the inner one should be formed during 1-day inhibition stage. Moreover, it seems that the ferrite uniformly corroded during pre-corrosion stage, however, ferrite corroded further only partially during the inhibition stage. This observation will be discussed in detail in following section. After 2-day pre-corrosion and 3-day inhibition, a uniform corrosion morphology with a thicker Fe_3C layer was observed on the specimen surface, as shown in Figure 6c and 6f. The pre-corrosion and inhibition stages could not be distinguished from the cross-sectional SEM image, which indicated the loss of inhibition on the specimen. This observation is consistent with the result of corrosion rate evolution that the inhibition was completely lost at the end (Figure 5, 30 ppm_w).

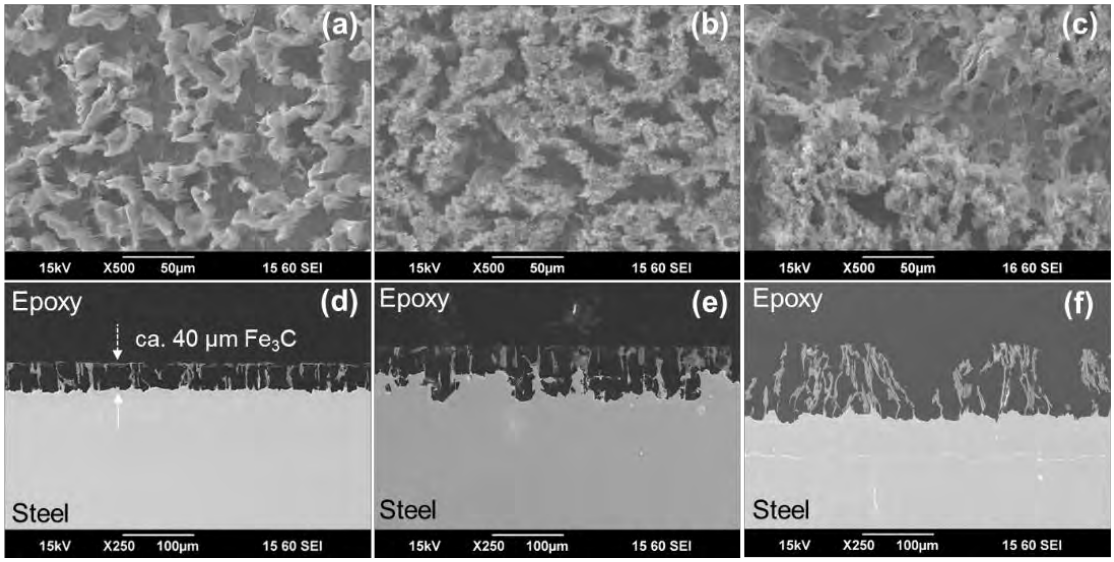

Figure 6: The top and cross-sectional view SEM images of C1018 specimens retrieved at different stages of the experiment in 50 g/L NaCl solution with 0.86 bar CO_2 at pH 4.5 and 55 °C with 30 ppm_w PE-C14. (a) and (d) from the specimen experienced 2-day pre-corrosion; (b) and (e) from the specimen experienced 2-day pre-corrosion and 1-day inhibition; (c) and (f) from the specimen experienced 2-day pre-corrosion and 3-day inhibition.

Further surface analyses were conducted to have a better understanding about the partial corrosion during the first day inhibition, as shown in Figure 7. Figure 7a demonstrates two corrosion stages, *i.e.*, 2-day pre-corrosion and 1-day inhibition, separated by white dashed lines in the image. The local corrosion rate at corroded site was estimated from the thickness difference to be around 12.8 mm/year, which was larger than the average corrosion rate around 8.0 mm/year measured by LPR in the first day of inhibition in Figure 5. Meanwhile, the other sites were protected with essentially no further corrosion after PE-C14 injection. To check whether the inhibited sites was related to certain microstructure of carbon steel, the cross-section of this specimen was etched using Nital to reveal the steel microstructure, as shown in Figure 7b. It demonstrated the ferrite and pearlite phases in the C1018. However, there was no connection between the microstructure and inhibition performance, which indicated that the protected sites during the inhibition stage were independent of phase distribution. Figure 7c shows the top view SEM image after Fe_3C layer was removed per ASTM G1[21], where many corroded valleys distributed across the surface without any preference.

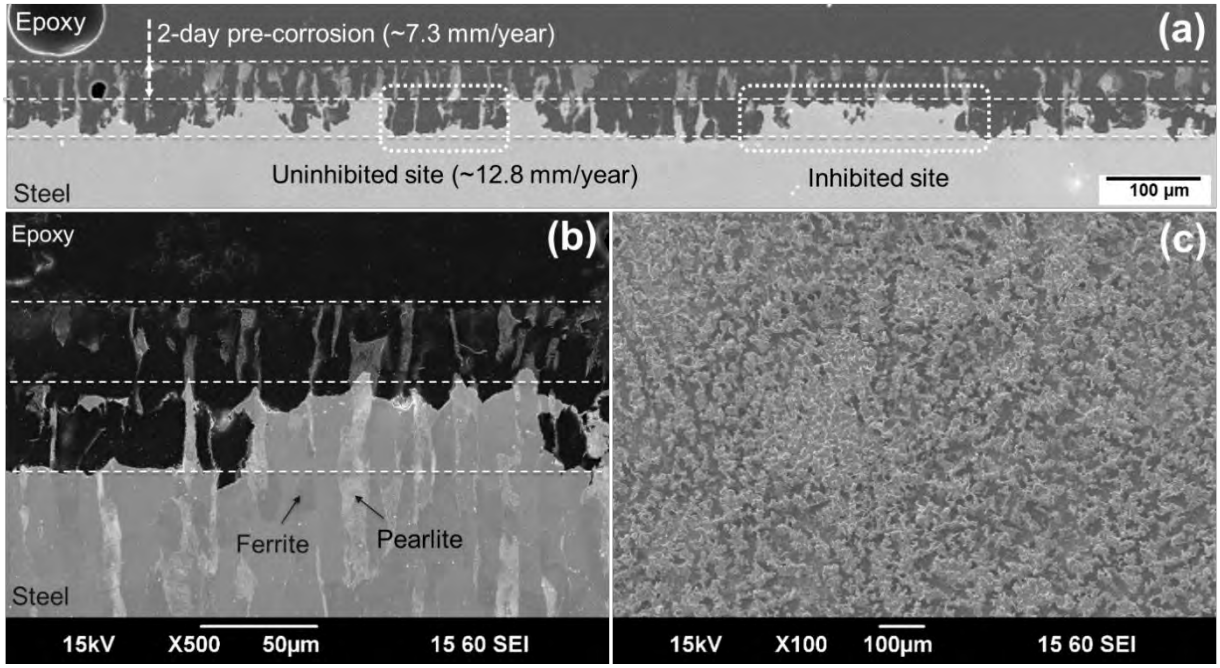

Figure 7: The cross-sectional and top view SEM images of C1018 specimens after 2-day pre-corrosion and 1-day inhibition from the experiment in 50 g/L NaCl solution with 0.86 bar CO_2 at pH 4.5 and 55 °C with 30 ppm_w PE-C14. (a) and (b) are cross-sectional view SEM images before and after etching; (c) is top view SEM image after removal of Fe_3C layer.

As aforementioned, the surface appearance of Fe_3C layer changed after 1-day inhibition with 30ppm_w compared with that after 2-day pre-corrosion only (Figure 6). In order to understand surface composition, the EDS was conducted at two sites on the specimen surface, as displayed in Figure 8. The first site is on the surface of Fe_3C and the second one is at steel bulk substrate surface. Their EDS spectra were shown in Figure 8b and 8c, respectively. A highly intense phosphorus peak was detected on Fe_3C surface, indicating that the adsorbed compound is very likely associated with PE-C14. According to previous evidence from EDS and Raman spectroscopy [10], the adsorbed compound could be separated PE-C14 or/and its complex with Fe^{2+} from solution due to "cloud point" effect. [22–25] However, spectrum detected at steel substrate showed no phosphorus enrichment. This implied that the PE-C14 preferred to accumulate on Fe_3C layer rather than at steel substrate. More experimental proof is required to validate this conclusion. The EDS mapping was collected from the cross-section of the same specimen shown in Figure 8d and 8e. A phosphorus-rich layer accumulated on the top of Fe_3C layer (Figure 8e), which should be the same as what was detected from the top of the specimen. Again, no measurable phosphorus accumulation was shown at the substrate of corroded or inhibited sites.

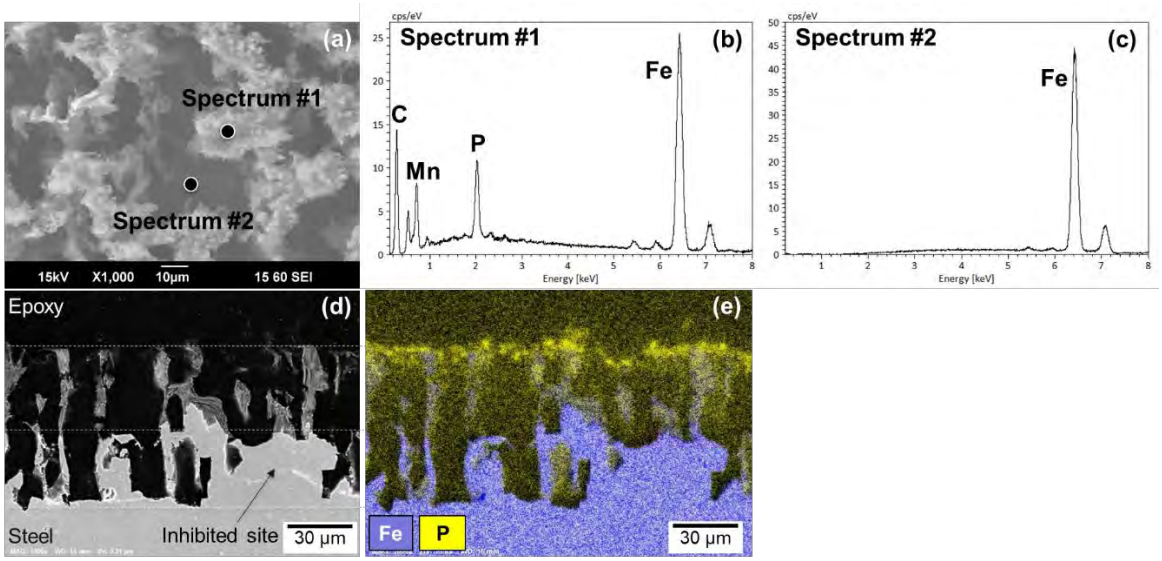

Figure 8: The EDS spectra at different surface sites and EDS mapping at cross-section of C1018 specimen after 2-day pre-corrosion and 1-day inhibition from the experiment in 50 g/L NaCl with 0.86 bar CO_2 at pH 4.5 and 55°C with 30 ppm_w PE-C14.

Inhibition with 300 ppm_w PE-C14.

The top view SEM images of C1018 specimen retrieved after 2-day pre-corrosion and 3-day inhibition with 300 ppm_w PE-C14 are shown in Figure 9Figure 10. PE-C14 associated compound cluster was found to cover the specimen surface at higher concentration (300 ppm_w). This physical coverage could reduce the limiting current of the hydrogen evolution reaction, which will be further discussed in below section. A similar surface morphology as that with 30 ppm_w was observed at uncovered sites.

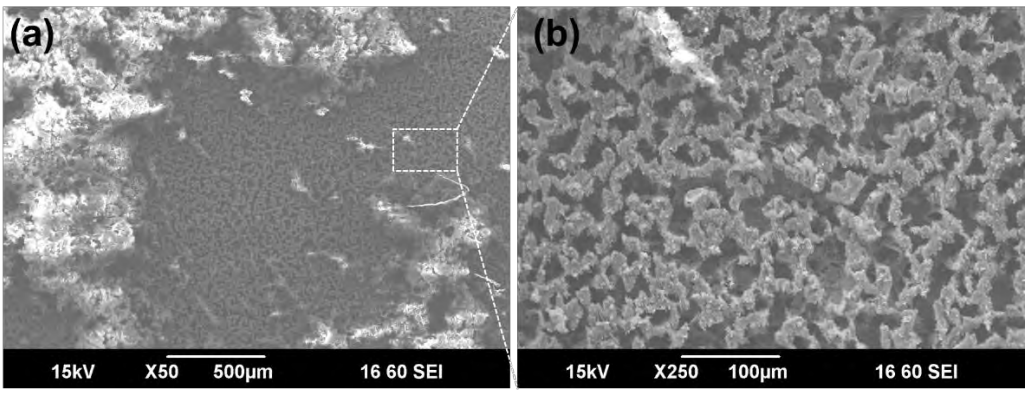

Figure 9: The top view SEM images of C1018 specimen retrieved after 2-day pre-corrosion and 3-day inhibition in 50 g/L NaCl with 0.86 bar CO_2 at pH 4.5 and 55°C with 300 ppm_w PE-C14.

The cross-sectional view SEM images of C1018 specimens retrieved at different stages of the experiment with 300 ppm_w PE-C14 are shown in Figure 10. The corrosion morphologies from cross-sectional view of all three specimens clearly showed two corrosion stages, *i.e.*, 2-day pre-corrosion stage and following inhibition stage. During 2-day pre-corrosion, a *ca.* 40 µm Fe_3C skeleton were revealed on the specimen surfaces with an estimated corrosion rate of 7.3 mm/year, which was consistent with the corrosion rate from weight loss measurement (7.6 mm/year). During inhibition stages, the surfaces were partially

corroded. After 1-day inhibition, the local corrosion rate at corroded site was around 8.8 mm/year (Figure 10a), which was lower than that (12.8 mm/year) in the case of 30 ppm_w PE-C14. This indicated that 300 ppm_w PE-C14 delivered more inhibition than 30 ppm_w, but still did not fully inhibit the substrate corrosion. As inhibition stage proceeded, the active corroding sites in the first day of inhibition was likely to further corrode and eventually develop into severe localized corrosion, as shown in Figure 10b and 10c. The corrosion rate at these sites was estimated to be around 10 mm/year, which was accelerated significantly *via* formation of a large cathodic area and small anodic area.

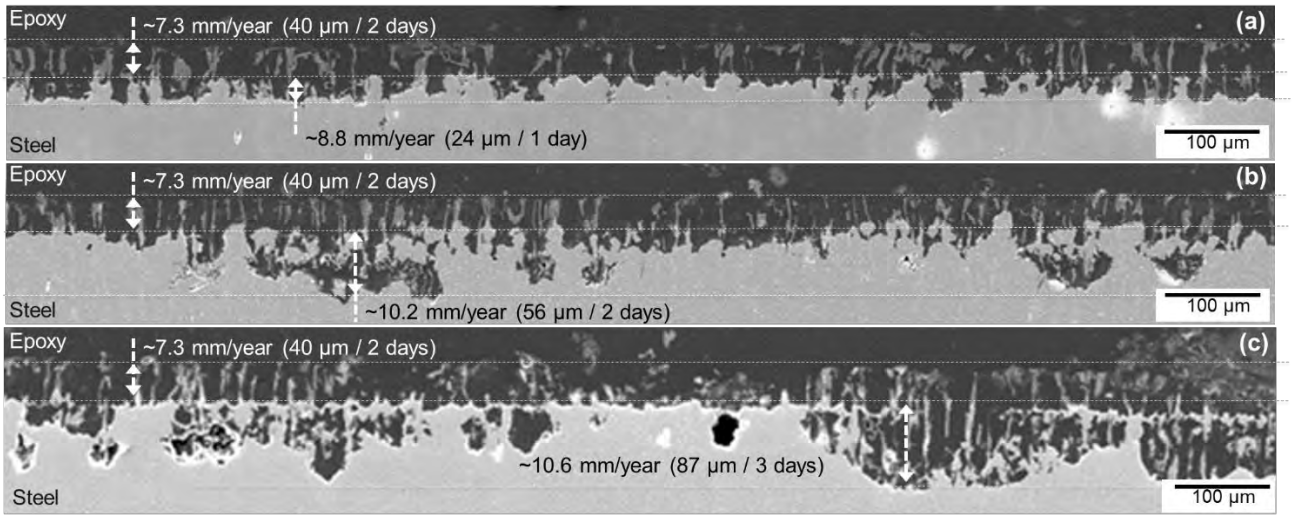

Figure 10: The cross-sectional view SEM images of C1018 specimens retrieved at different stages of the experiment in 50 g/L NaCl with 0.86 bar CO_2 at pH 4.5 and 55°C with 300 ppm_w PE-C14. (a) from the specimen experienced 2-day pre-corrosion and 1-day inhibition; (b) from the specimen experienced 2-day pre-corrosion and 2-day inhibition; (c) from the specimen experienced 2-day pre-corrosion and 3-day inhibition.

Potentiodynamic Polarization Curve Analysis

The potentiodynamic polarization curves of C1018 specimen collected from the experiments in the studied condition at 55°C with both 30 and 300 ppm_w PE-C14 are displayed in Figure 11. Before injecting PE-C14, the limiting current of hydrogen ion reduction reaction was significantly increased after 2-day pre-corrosion, resulting from the exposed Fe_3C layer serving as additional cathodic reaction area. For the same reason, the charge transfer controlled part of hydrogen reduction was expected to be accelerated to the same extent, which could not be seen from the polarization curves since the cathodic reaction was under mass transfer control. The slight retardation on anodic reaction could be due to the change of local environment, such as the accumulation of ferrous ion. After 2-day pre-corrosion and 1-day inhibition with 30 ppm_w PE-C14, the anodic reaction showed no retardation compared with 2-day pre-corrosion only, suggesting that the inhibition mainly resulted from the retardation on cathodic reaction. After 2-day pre-corrosion and 4-day inhibition with 300 ppm_w PE-C14, the anodic reaction was retarded, and the cathodic reaction was expected to be retarded as well, compared with 2-day pre-corrosion only. However, the retardation on anodic reaction was very limited compared with the case of no pre-corrosion and 4-day inhibition. These results were consistent with corrosion rate results, suggesting 300 ppm_w PE-C14 was still not enough to inhibit the corrosion rate of 2-day pre-corroded C1018 to a low level (0.1 mm/year). Besides, it is worthy to point out that the hydrogen limiting current decreased in the presence of 300ppm_w PE-C14, and this was due to the precipitated PE-C14 or/and its complex with Fe^{2+} covering on the specimen surface and forming a diffusion barrier.

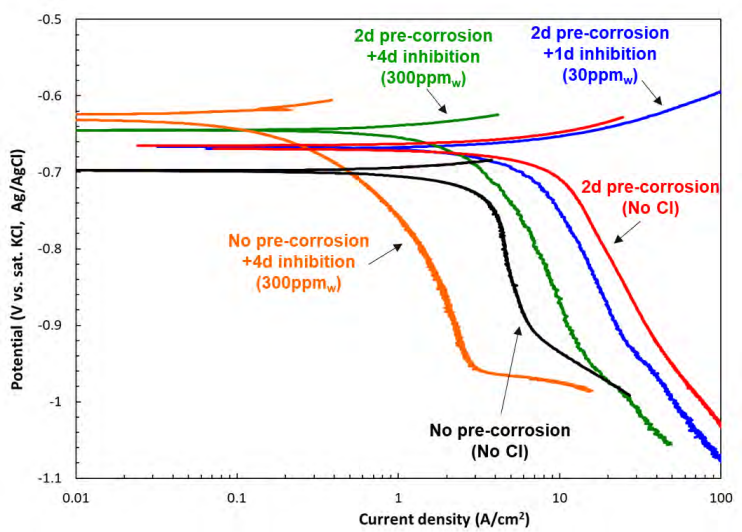

Figure 11: The potentiodynamic polarization curves of C1018 specimen collected from the experiments in 50 g/L NaCl with 0.86 bar CO_2 at pH 4.5 and 55°C with both 30 and 300 ppm_w PE-C14.

Discussion

The presence of 300 ppm_w PE-C14 showed a higher inhibition efficiency than that with 30 ppm_w indicated by a lower stabilized corrosion rate, a larger protected surface area, and enhanced retardation on electrochemical reactions. This clearly indicates that the inhibition performance is highly dependent upon the bulk concentration of the CI. In the tested conditions, 300 ppm_w PE-C14 could still not inhibit the corrosion rate in the presence of a *ca.* 40 µm Fe_3C layer to a level comparable to specimens that did not undergo pre-corrosion (0.1 mm/year), even though it was at least 15 times higher than the surface saturation concentration [7, 8, 10] of PE-C14 on bare steel. This result implies a higher concentration will be needed to achieve an acceptable inhibition efficiency in the presence of a Fe_3C layer, which is consistent with many other studies.[2, 3]

Under the tested conditions, the lower inhibition efficiency in presence of 40 µm of Fe_3C skeleton was due to the significant acceleration of the corrosion rate by the significantly increased cathodic reaction area from the exposed Fe_3C layer. However, it is fair to question whether such a thick Fe_3C layer can maintain in the field over longer period time, especially considering that C1018 is not commonly used for pipelines. In terms of the inhibition of anodic reaction, the less retardation compared with bare surface could be related to the change of local solution environment, which made the CI adsorption at the substrate more difficult, such as the accumulation of ferrous ion therein. As for the inhibition of cathodic reaction, residual Fe_3C skeleton massively increased cathodic area required to be inhibited by the adsorption of PE-C14. This could decrease the bulk concentration of PE-C14, hence, impairing inhibition efficiency. It is also anticipated that this bulk concentration dependency is due to the experimental configuration where depletion of bulk concentration is possible by adsorbing at various interfaces. Indeed, the CI was injected in one single shot in a closed system, whereas CI are continuously injected in real field conditions. In addition, specifically for the tested model CI compound PE-C14, its bulk concentration could be consumed more significantly by the complexation with corrosion-released Fe^{2+} since the releasing rate was accelerated in the presence of a Fe_3C layer. Unfortunately, the concentration of PE-C14 was not monitored in this work due to the difficulty in measuring phosphate ester type CI.

More related works have been conducted to address the limitations of this work and shed light on the inhibition mechanism in the presence of residual Fe_3C. In our ongoing work, the detrimental effect of residual Fe_3C on corrosion inhibition was evaluated on mild steels with different microstructures and carbon contents. The corrosion inhibitor was also continuously injected into the testing glass cell and the CI concentration was monitored throughout the experiments. Both short-term and long-term experiments were conducted to study the role of exposure duration. Promising results have been obtained and will be discussed in our future publications.

CONCLUSIONS

A *ca.* 40 μm Fe_3C skeleton exposed after 2-day pre-corrosion significantly accelerated the corrosion rate and limiting current of the hydrogen reduction reaction *via* serving as additional cathodic reaction sites. Considering this layer, 300 ppm_w CI model compound PE-C14 did not inhibit the corrosion rate to a level comparable to that on a bare surface (0.1 mm/year), even though its concentration was at least 15 times higher than the surface saturation concentration on bare steel. The inhibition in the presence of Fe_3C was mainly from the retardation of cathodic reaction. Less retardation of anodic reaction compared with that on bare steel could be related to the change of local solution environment, such as ferrous ion accumulation. After injecting PE-C14, a non-uniform corrosion morphology was observed on specimens with 2-day pre-corrosion, which was postulated to promote localized attack in the case of 300 ppm_w PE-C14.

These results should be considered with great cautiousness due to the following limitations of present work.

- The residual Fe_3C maintained on steel surface after pre-corrosion is microstructure dependent and usually mechanically weak. Its detrimental effect on corrosion inhibition varies with different steel types and flow conditions. The current results are only validated with C1018 steel with ferritic-pearlitic microstructure and applied flow condition.

- The corrosion inhibitor is continuously injected into the pipeline and a constant concentration will be usually maintained. However, the current work was conducted in a closed glass cell with one shot injection of a limited volume, which could result in the depletion of bulk CI concentration due to adsorption on the porous Fe_3C residue and other interfaces. Specifically for PE-C14 model compound, the complexation effect with corrosion-released ferrous ion would deplete its concentration even further.

More related works have been conducted to address the raised questions along the various findings and will be discussed in future publications.

ACKNOWLEDGEMENTS

This project has been supported by TotalEnergies transversal R&D project (MANA Project). The authors would like to thank TotalEnergies for their financial support.

REFERENCES

1. G. Koch, J. Varney, N. Thopson, O. Moghissi, M. Gould, and J. Payer, “International measures of prevention, application, and economics of corrosion technologies study,” in NACE International, 2016, pp. 1–216.

2. E. Gulbrandsen, S. Nesic, A. Stangeland, T. Burchardt, B. Sundfaer, S. M. Hesjevik, and S. Skjerve, “Effect of precorrosion on the performance of inhibitors for CO_2 corrosion of carbon steel,” CORROSION 1998, paper no. 98013 (Houston, TX: NACE, 1998).

3. Y. Xiong, D. Fischer, F. Cao, and J. Pacheco, “Impact of pre-corrosion on corrosion inhibitor performance: Can we protect aged pipelines,” CORROSION 2017, paper no. 8919 (Houston, TX: NACE, 2017).

4. H. H. Zhang, X. Pang, M. Zhou, C. Liu, L. Wei, and K. Gao, “The behavior of pre-corrosion effect on the performance of imidazoline-based inhibitor in 3 wt.% NaCl solution saturated with CO_2,” Appl. Surf. Sci., vol. 356, pp. 63–72, Nov. 2015.

5. L. D. Paolinelli, T. Pérez, and S. N. Simison, “The effect of pre-corrosion and steel microstructure on inhibitor performance in CO_2 corrosion,” Corros. Sci., vol. 50, no. 9, pp. 2456–2464, Sep. 2008.

6. H. Yu, J. H. Wu, H. R. Wang, J. T. Wang, and G. S. Huang, “Corrosion inhibition of mild steel by polyhydric alcohol phosphate ester (PAPE) in natural sea water,” Corros. Eng. Sci. Technol., vol. 41, no. 3, pp. 259–262, Sep. 2006.

7. Y. He, S. Ren, X. Wang, D. Young, M. Singer, Z. Belarbi, M. Mohamed-Saïd, S. Camperos, M. R. Khan, and K. Cimatu, “Delinkage of Metal Surface Saturation Concentration and Micellization in Corrosion Inhibition,” Corrosion, vol. 78, no. 7, pp. 625–633, Jul. 2022.

8. S. Ren, Y. He, Z. Belarbi, X. Wang, D. Young, M. Singer, M. Mohamed-Said, and S. Camperos, “Methodology of Corrosion Inhibitor Characterization Applied to Phosphate Ester and Tetrahydropyrimidinium Model Compounds,” in AMPP CORROSION Virtual Conference + Expo, 2021, paper no. 16443 (Houston, TX: AMPP, 2021).

9. Y. He, S. Ren, Z. Belarbi, X. Wang, D. Young, and M. Singer, “Micellization and Inhibition Efficiency,” in AMPP CORROSION Virtual Conference + Expo, 2021, paper no. 16872 (Houston, TX: AMPP, 2021).

10. S. Ren, Y. He, X. Wang, D. Young, M. Singer, M. Mohamed-Saïd, and S. Camperos, “The Change of Corrosion Inhibition Behavior of Tetradecyl Phosphate Ester at Elevated Temperatures,” in AMPP Annual Conference+Expo 2022, paper no. 18053 (Houston, TX: AMPP, 2022).

11. Y. He, S. Ren, X. Wang, D. Young, M. Singer, M. Mohamed-Saïd, and S. Camperos, “The Effect of Temperature on the Adsorption Behavior and Inhibition Performance of a Pyrimidine-Type Inhibitor at Medium Temperature Range (25°C to 80°C),” in AMPP Annual Conference+Expo 2022, paper no. 17895 (Houston, TX: AMPP, 2022).

12. X. Wang, S. Ren, Y. He, D. Young, M. Singer, M. Mohamed-Said, and S. Camperos, “Effect of Organic Solvent on Corrosion Inhibition of Mild Steel in CO_2 Environment,” in AMPP Annual Conference+Expo 2022, paper no. 17942 (Houston, TX: AMPP, 2022).

13. H. Mansoori, D. Young, B. Brown, S. Nesic, and M. Singer, “Effect of $CaCO_3$-saturated solution on CO_2 corrosion of mild steel explored in a system with controlled water chemistry and well-defined mass transfer conditions,” Corros. Sci., vol. 158, p. 108078, Sep. 2019.

14. H. Mansoori, B. Brown, D. Young, S. Nešić, and M. Singer, “Effect of $FexCayCO_3$ and $CaCO_3$ Scales on the CO_2 Corrosion of Mild Steel,” Corrosion, vol. 75, no. 12, pp. 1434–1449, Dec. 2019.

15. H. Mansoori, D. Young, B. Brown, S. Nesic, and M. Singer, “Effect of $CaCO_3$-saturated solution on CO_2 corrosion of mild steel explored in a system with controlled water chemistry and well-defined mass transfer conditions,” Corros. Sci., vol. 158, p. 108078, Sep. 2019.

16. M. C. Di Bonaventura, B. Brown, and M. Singer, “Removal of Iron Carbide in Turbulent Flow Conditions and Influence of Iron Carbonate Formation in Aqueous CO_2 Corrosion of Mild Steel,” Corrosion, vol. 78, no. 10, pp. 970–977.

17. B. A. Alink, B. Outlaw, V. Jovancicevic, S. Ramachandran, and S. Campbell, “Mechanism of CO_2 Corrosion Inhibition by Phosphate Esters,” CORROSION 1999, paper no. 99037 (Houston, TX: NACE, 1999).

18. R. Nyborg, E. Gulbrandsen, T. Loeland, and K. Nisancioglu, “Effect of steel microstructure and composition on inhibition of CO2 corrosion,” CORROSION 2000, paper no. 00023 (Houston, TX: NACE, 2000).

19. F. Farelas, B. Brown, and S. Nesic, “Iron carbide and its influence on the formation of protective iron carbonate in CO_2 corrosion of mild steel,” CORROSION 2013, paper no. 2291 (Houston, TX: NACE, 2013).

20. M. Di Bonaventura, B. Brown, S. Nešić, and M. Singer, “Effect of Flow and Steel Microstructure on the Formation of Iron Carbonate,” CORROSION, vol. 75, no. 10, pp. 1183–1193, Oct. 2019.

21. ASTM G1-90, “ASTM G1 Standard Practice for Preparing, Cleaning, and Evaluation Corrosion Test Specimens,” ASTM, 1999.

22. W. N. Maclay, “Factors affecting the solubility of nonionic emulsifiers,” J. Colloid Sci., vol. 11, no. 3, pp. 272–285, Jun. 1956.

23. A. M. Al-Ghamdi and H. A. Nasr-El-Din, “Effect of oilfield chemicals on the cloud point of nonionic surfactants,” Colloids Surfaces A Physicochem. Eng. Asp., vol. 125, no. 1, pp. 5–18, May 1997.

24. K. S. Sharma, S. R. Patil, and A. K. Rakshit, “Study of the cloud point of C12En nonionic surfactants: effect of additives,” Colloids Surfaces A Physicochem. Eng. Asp., vol. 219, no. 1–3, pp. 67–74, Jun. 2003.

25. P. D. T. Huibers, D. O. Shah, and A. R. Katritzky, “Predicting Surfactant Cloud Point from Molecular Structure,” J. Colloid Interface Sci., vol. 193, no. 1, pp. 132–136, Sep. 1997.